sciendo
Polish Journal of Medical Physics and Engineering
The Journal of Polish Society of Medical Physics
ISSN 1898-0309, doi: 10.2478/pjmpe-2024-0023
December 2024
Vol 30, Issue 4

Scientific Paper

Investigation of the effectiveness of eight different metal artifact reduction algorithms in reducing extracorporeal metal artifacts: a phantom study using the Gumbel method

Keiko SUZUKI[1,2,ABCDEF,*], Hiroe MUTO[1,2,ABCDEF]
[1]*Graduate School of Health Science, Suzuka University of Medical Science, Suzuka-city, Mie, Japan*
[2]*Department of Radiological Technology, Faculty of Health Science, Suzuka University of Medical Science, Suzuka-city, Mie, Japan*
[*]*Corresponding author: Keiko Suzuki; lingmu0329@hotmail.co.jp*

(received 3 June 2024; accepted 30 July 2024)

Abstract
Introduction: Metal Artifact Reduction (MAR) processing has been clinically applied to computed tomography (CT) images using various methods. Iterative MAR (iMAR) is an algorithm for reducing metal artifacts from implants and is tailored to the type, shape, and imaging site of a metal object. Various implants have been targeted using iMAR; however, there are some implants and metals that do not have a dedicated iMAR. The potential of iMAR for managing such artifacts has not yet been explored. Utilizing iMAR in unavoidable extracorporeal metal artifact cases could improve diagnosis. We aimed to assess whether the iMAR reduces extracorporeal metal artifacts and enhances image quality.
Material and methods: CT was performed on a whole-body phantom with electrocardiogram (ECG) electrodes attached. Images were obtained without the iMAR and with eight different iMAR processings. The CT value profiles were perpendicular to the direction of artifact generation, and the maximum adjacent CT value difference was extracted from each CT value profile as the largest variation. The cumulative probabilities for the largest variations were obtained, and the location and scale parameters were calculated from the cumulative probability plots. Kruskal–Wallis tests and multiple comparisons were performed on nine different images.
Results: Regarding the 100 cumulative probability plots of the largest variations obtained from each CT value profile, the coefficients of determination (R^2) for all cumulative probability plots were as high as > 0.84, indicating that the features of the extracorporeal metal artifact generated from the ECG electrodes evaluated in this study asymptotically approached a Gumbel distribution. The location parameters showed no significant differences among the nine processed images ($p > 0.11$), whereas the scale parameters showed significant differences for neuro coil, shoulder implant, extremity implant, and thoracic coil iMAR-processed images compared with controls ($p < 0.05$).
Conclusion: iMAR may improve diagnosis by reducing extracorporeal metal artifacts and enhancing image quality.

Keywords: computed tomography; Gumbel distribution; metal artifact reduction.

Introduction

In computed tomography (CT) images, shadows that do not naturally exist within the subject or the image may appear because of various factors, such as the subject itself, acquisition of projection data, and image reconstruction. These problematic shadows are collectively known as artifacts, which can cause inaccurate CT values and interfere with diagnosis. Measures to suppress these effects have been implemented in CT devices.[1] Artifacts caused by internal metals are among the factors that degrade image quality. Recently, metal artifact reduction (MAR) processing techniques using different completion processing methods have been applied clinically.[2-5] Compared with images reconstructed using the filtered back projection (FBP) method, those that undergo MAR processing, which reduces artifacts, have higher image quality.[2,6-8] Furthermore, artifacts are effectively reduced in images that undergo MAR processing compared with those processed using iterative reconstruction alone,[9,10] and the usefulness of MAR processing has been reported in many cases, both in Japan and overseas.[2-4,6-16]

The iterative MAR (iMAR) process (Siemens Healthcare, Erlangen, Germany) is a MAR algorithm developed based on the sinogram inpainting method. The iMAR recovers the metal information in the sinogram that is lost in the CT image. In addition, it can select an optimized algorithm depending on the

Authors' contribution: A – Research concept and design, B – Collection and/or assembly of data, C – Data analysis and interpretation, D – Writing the article, E – Critical revision of the article, F – Final approval of the article.

type of metallic implant to be targeted, the type of artifact, and the imaging site, making it possible to respond to various clinical conditions. The iMAR technology has been used to target several types of implants in the body; however, its use on other implants and metals remains unexplored.

The artifact reduction effects of iMAR on non-targeted metal implants have been reported in a previous study,[7] and improved image quality achieved using other algorithms, despite the existence of a dedicated iMAR algorithm, has been reported in another study,[11] suggesting that iMAR can also be used on other objects. There are currently no reports on the use of the iMAR for extracorporeal metal artifacts; however, based on our interpretation of previous studies, we suspect that there may be iMAR algorithms that can be applied to extracorporeal metal artifacts.

In clinical practice, depending on the patient's condition, examinations and interventions, such as examinations for emergency patients or the use of life-sustaining medical devices, are performed without removing metal-containing objects from the body. The images acquired in such cases are slightly disadvantageous. In addition, re-examination and re-scanning may increase patient and surgeon exposure. If iMAR can be used in cases in which extracorporeal metal artifacts are unavoidable, it can be used in a broader range of applications; in diagnostic imaging, iMAR can help reduce stress on the reader by improving image quality and diagnosis. Therefore, a search for more possibilities of using iMAR is required.

In this study, we aimed to determine the effects of different iMAR algorithms on artifact reduction for extracorporeal metal artifacts in CT images.

Materials and methods

Study design

This was a phantom-based study and was therefore exempt from ethical review.

Image acqusition

We used a 128-detector multi-slice CT scanner (Somatom Definition AS+; Siemens Healthcare, Erlangen, Germany). Electrocardiogram (ECG) electrodes (Siemens Healthcare, Erlangen, Germany) were affixed to the trunk of a whole-body phantom (PBU-60; Kyoto Kagaku, Kyoto, Japan) as a source of metal artifacts for CT (**Figure 1**). The metal part of the ECG electrode was made of copper and nickel alloy. CT images were acquired under clinically used thoracic and abdominal scanning conditions: tube voltage of 120 kV, automatic tube current-time product, and rotation time of 0.5 s. Image reconstruction was performed using a field of view of 320 mm, slice thickness of 1 mm, reconstruction interval of 1 mm, reconstruction function B36f, and the customarily used FBP method. Ten consecutive slices with artifacts were acquired and used as control images. Image reconstruction was then performed on the control images using eight different iMARs, including neuro coils, shoulder implants, extremity implants, thoracic coils, hip implants, pacemakers, spine implants, and dental fillings.

Selection of artifact evaluation method

In previous studies, visual score evaluation and the standard deviation (SD) of CT values were used to evaluate the uniformity of CT images when assessing metal artifacts.[7,12] Visual evaluation alone is not objective, and evaluation using SD combines potential image noise and artifacts, making it difficult to evaluate artifacts alone. The recent artifact evaluation methods include the Artifact Index (AI)[15-17] and the Gumbel method.[17-25] The AI evaluation is based on the SD of CT values and involves removing noise from artifact images. However, a noise image without artifacts is required to remove noise, making it difficult to apply the AI method in clinical practice. The Gumbel method focuses on the difference between the distribution of normally distributed noise and artifacts that follow a Gumbel distribution and can theoretically evaluate only artifacts.[20] This suggests that the method can be applied to clinical images. Therefore, as a quantitative evaluation method for artifacts, we calculated quantitative values in the present study using the Gumbel method devised by Imai et al.[18]

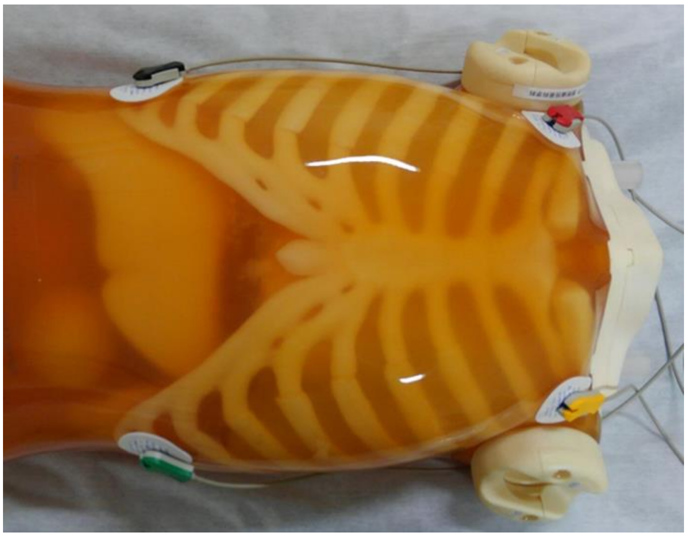

Figure 1. Phantom and ECG Electrode Affixing Diagram

Calculation of quantitative value of artifacts using the Gumbel method

The artifacts were evaluated using the Gumbel method, as described previously.[18] A slice of the acquired image is shown in **Figure 2a**. First, a 40 × 100-pixel rectangular region of interest (ROI) was set in ImageJ, as shown in **Figure 2b**, to obtain 100 CT value profiles of 40-pixel length in the depth direction, which were drawn perpendicular to the direction of artifact generation on the image, and CT values were obtained.

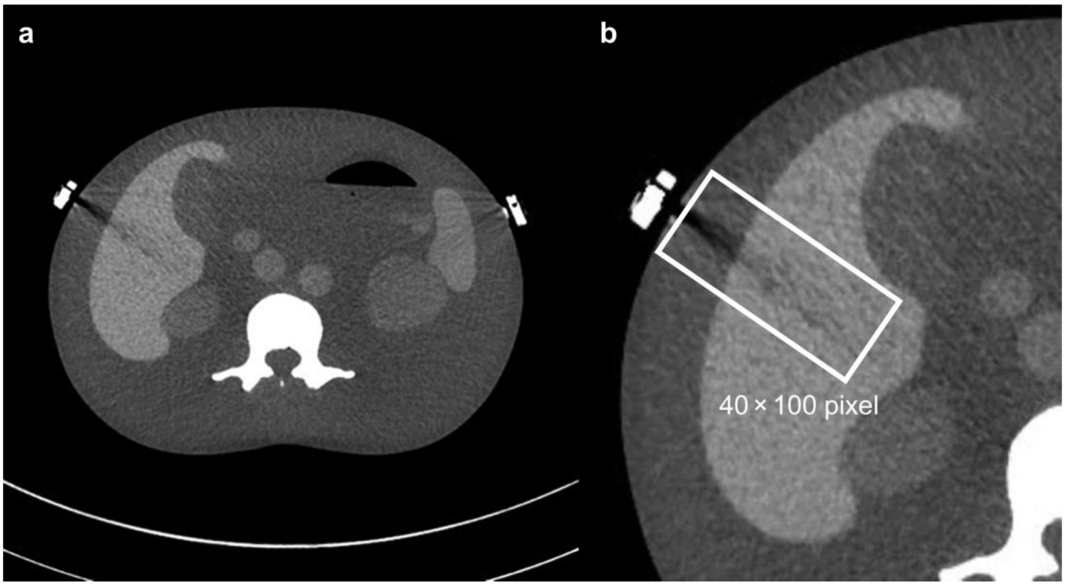

Figure 2. Acquired image (control image). a. One slice of ten acquired images (control image), b. Position of the ROI setting

Subsequently, the maximum value was extracted from the CT value differences between adjacent pixels in a 40-pixel-long CT value profile. The maximum value was defined as the largest variation. Similarly, the largest variation for each of the 100 CT value profiles in the depth direction of the artifact was obtained. A cumulative probability distribution chart was created by determining the cumulative probability for the 100 largest variations; then, the location and scale parameters, which are quantitative values, were obtained from the graph. Image J 1.52a (NIH) was used for image analysis.

The Gumbel method

In the Gumbel method, the CT value profile is first obtained perpendicular to the direction of artifact generation. This artifact causes the greatest variation in the CT values in this CT value profile. Therefore, the largest variation for each CT value profile was extracted as an artifact feature. Generally, the maximum random variable in a sample drawn from a population has been shown to follow an extreme-value distribution, and of the three distributions (Gumbel, Frechet, and Weibull distributions), artifacts are reported to be asymptotic to the Gumbel distribution.[18] The Gumbel distribution is defined as follows:

$$F(x) = exp\left[-exp\left(-\frac{x-\beta}{\gamma}\right)\right] \quad \text{Eq. 1}$$

F(x): cumulative probability for random variable x
β: location parameter
γ: scale parameter

The cumulative probability is obtained using the Mean Rank method.[18]

$$F(xi) = \frac{i}{n+1} \quad \text{Eq. 2}$$

F(xi): cumulative probability for the i-th largest random variable *xi*
n: number of samples

The location parameter *β* represents the upper or lower limit that the random variable can take, whereas the scale parameter *γ* represents the range, or variability, that the random variable can take. The location and scale parameters were obtained by performing a double logarithmic transformation on the Gumbel-defined equation.

$$-\ln\{-(\ln F(x))\} = \frac{1}{\gamma}x - \frac{\beta}{\gamma} \quad \text{Eq. 3}$$

The scale parameter can be calculated from slope *a* of the relationship $y = ax + b$, which is expressed by the linear equation shown in **Equation 3**, whereas the location parameter can be calculated from slope *a* and intercept *b*.

$$\gamma = \frac{1}{a} \quad \text{Eq. 4}$$

$$\beta = -\frac{b}{a} \quad \text{Eq. 5}$$

In the present study, the location and scale parameters were used as quantitative values for the evaluation of the artifacts.

Statistical analysis

The calculated location and scale parameters were compared among the nine groups in the control image and the eight iMAR-processed images. Statistical analysis was performed using EZR (R-Vers. 2.6-1). The Kruskal–Wallis test was used for significance difference tests, and the Steel method was used for multiple comparisons.

Results

A control image and eight different iMAR images are shown in **Figure 3**. **Figure 3a** shows a control image without iMAR, whereas **Figures 3b-i** show images reconstructed using eight different iMAR algorithms.

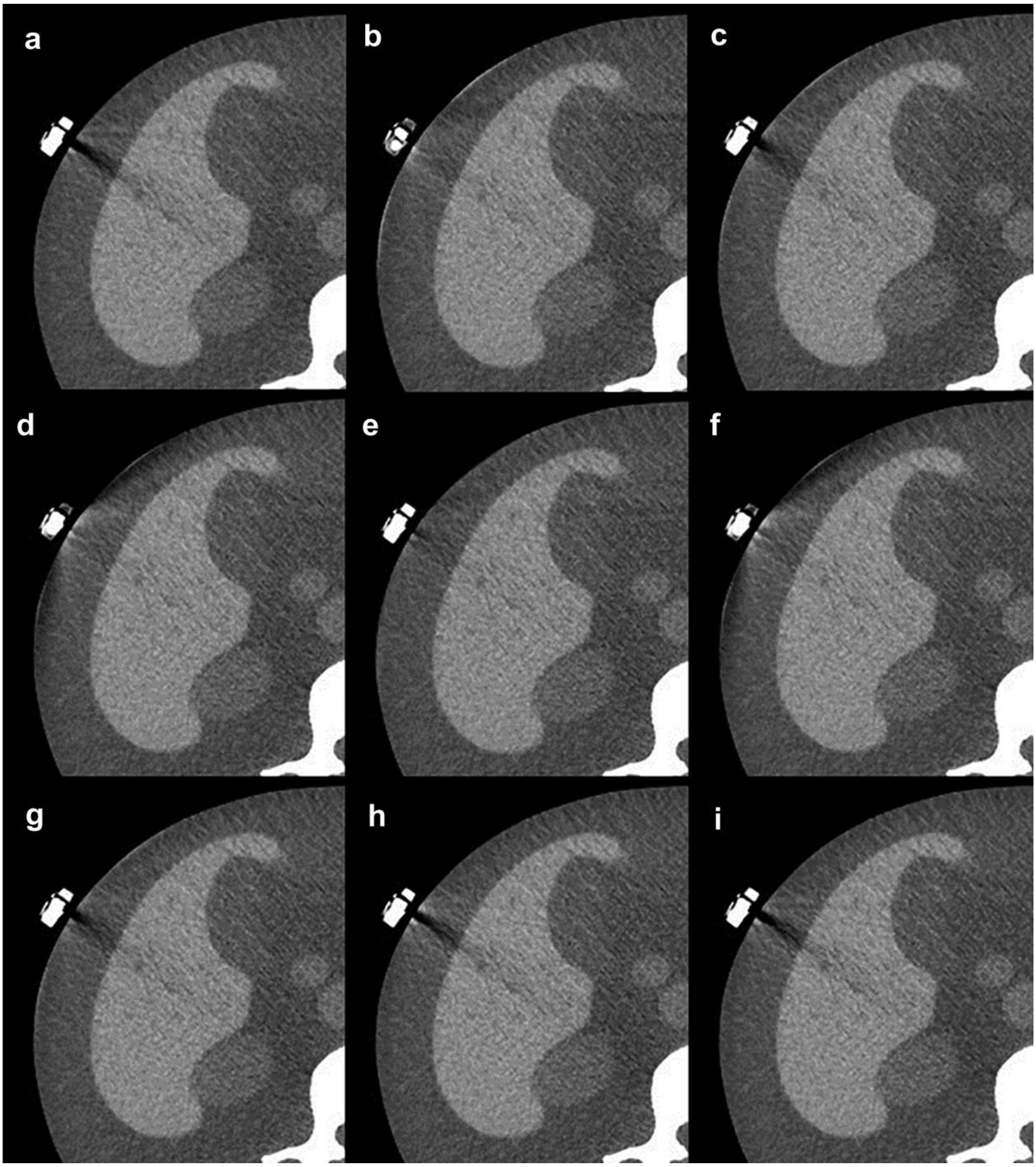

Figure 3. Examples of control and iMAR processed images. a. non-iMAR image (control image), b. neuro coils, c. shoulder implants, d. extremity implants, e. thoracic coils, f. hip implants, g. pacemaker, h. spine implants, i. dental fillings

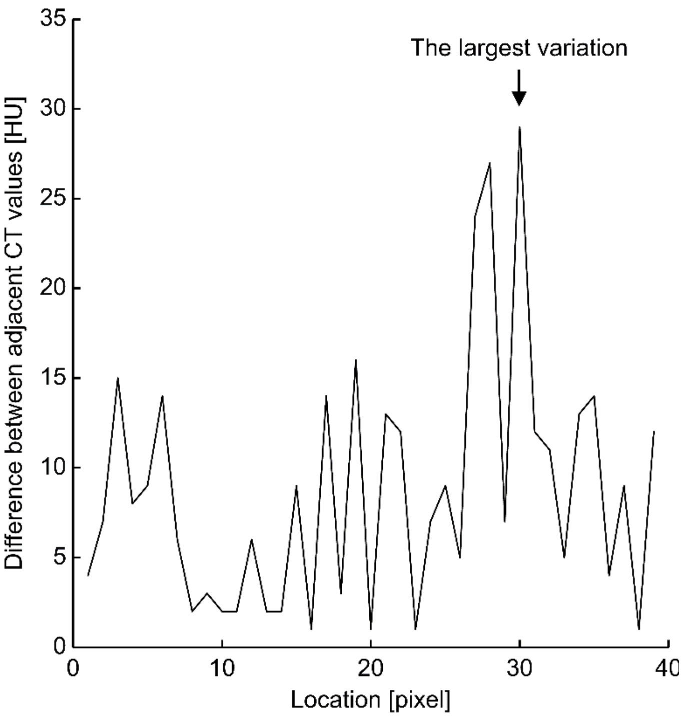

Figure 4. CT value differences between adjacent pixels in the CT value profile

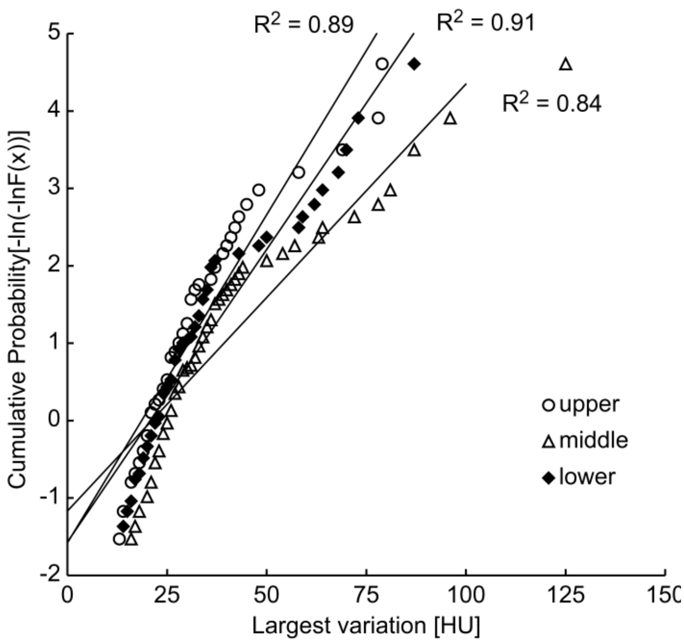

Figure 5. Gumbel Plot - Cumulative probability distribution plots for the largest variation

An example plot of the CT value differences between adjacent pixels based on a 40-pixel-long CT value profile is shown in **Figure 4**. The maximum value in the graph was extracted as the largest variation. **Figure 5** shows the plot results of the cumulative probability of the largest variation extracted from 100 CT value profiles acquired similarly in the depth direction of the artifact.

The graph shows a plot of the cumulative probability against the largest variation for the first (upper), fifth (middle), and tenth (lower) slices from the head side of the 10 acquired images. The coefficients of determination for each of the three images with different slice positions were calculated as $R^2 > 0.84$, indicating a strong fit to the approximation curve. Therefore, the features of the metal artifacts generated from the ECG electrodes evaluated in the present study asymptotically approached the Gumbel distribution.

The median values of the location and scale parameters calculated using the Gumbel method from the control images and the images processed using each iMAR algorithm are presented in **Table 1**.

Table 1. Location and scale parameters

Type of iMAR		location parameter	scale parameter
non-iMAR	1 Control images	22.17	13.57
iMAR+	2 Neuro coils	21.03	5.19
	3 Shoulder implants	22.84	7.12
	4 Extremity implants	21.93	5.91
	5 Thoracic coils	22.85	8.00
	6 Hip implants	22.01	7.55
	7 Pacemaker	23.05	8.83
	8 Spine implants	24.74	12.76
	9 Dental fillings	24.43	12.78

A Kruskal-Wallis tests and Steel's multiple comparisons as post-hoc tests were performed to determine if there were significant differences in the location and scale parameters obtained from the 10 processed images. The location parameters were not significantly different between the images ($p > 0.11$), whereas the scale parameters significantly differed ($p < 0.05$). The results are presented in **Table 2** and **Figure 6**.

The analysis results showed that the scale parameters were significantly lower in the iMAR-processed images of the neuro coils, shoulder implants, extremity implants, and thoracic coils than in the control images.

Discussion

In clinical practice, depending on the patient's condition, there are cases in which examinations and interventions must be performed without removing metal-containing objects from the body, resulting in artifacts in the images. In the present study, we compared the location and scale parameters of nine different CT images with extracorporeal metal artifacts; that is, images processed using eight different iMAR algorithms and those without iMAR processing. The results showed no significant differences in the location parameters among the images. Significant differences in the scale parameters were observed in images processed with four (neuro coil, shoulder implant, extremity implant, and thoracic coil) of the eight iMAR algorithms compared with control images, indicating a smaller scatter of artifacts. Therefore, the use of these four iMAR algorithms was effective in reducing the artifacts generated from the ECG electrodes attached outside the body.

In the present study, the iMAR was applied to extracorporeal metal artifacts that were not covered by the iMAR algorithm. In previous studies in which the dedicated MAR algorithm for specific implants was compared with other MAR algorithms, improved image quality was observed, even when other algorithms were used,[11] and MAR algorithms that improved image quality for implants without a corresponding MAR algorithm were reported.[7] Consistent with previous studies, the present study also revealed reduced artifacts when four different non-targeted iMAR algorithms were used. It is difficult to examine the iMAR algorithm in detail because it has only been partially disclosed; however, the neuro coil algorithm may have been effective in reducing artifacts because of the similarity in the size of the metal part of the ECG electrodes and the artifacts it generates. For the shoulder and extremity implant algorithms, the metal artifact shape was completely different from that of the ECG electrodes' however, similarities in the shape and intensity of the artifacts suggested that both algorithms were also effective in reducing artifacts. Regarding the thoracic coil algorithm, the size of the metal is similar to that of the ECG electrode in terms of the coil; however, because the background organs differ, the difference in the pattern of artifact generation is considered not to have led to the same reduction effect as that

Table 2. Multiple comparisons of scale parameters using the steel method

Multiple comparisons	p value
Control images : Neuro coils	0.002 (<0.05)
Control images : Shoulder implants	0.010 (<0.05)
Control images : Extremity implants	0.013 (<0.05)
Control images : Thoracic coils	0.041 (<0.05)
Control images : Hip implants	0.051
Control images : Pacemaker	0.051
Control images : Spine implants	1.00
Control images : Dental fillings	1.00

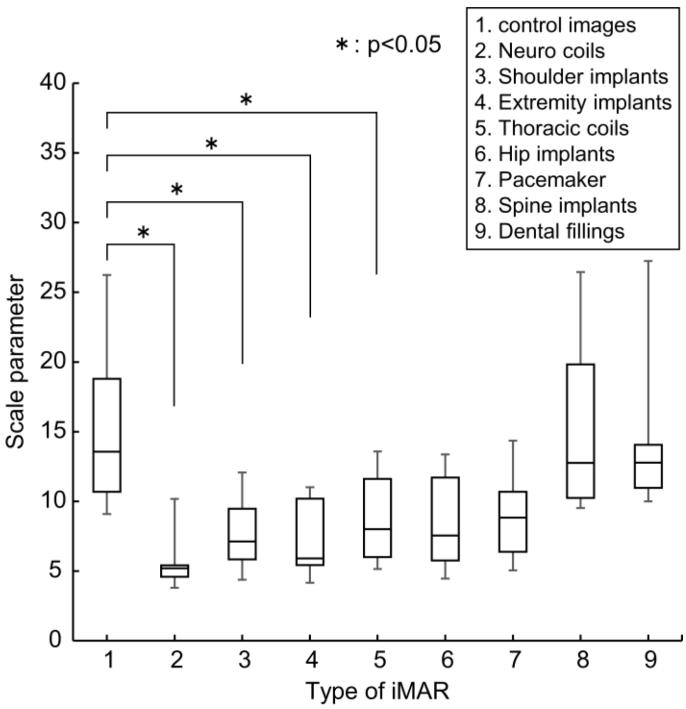

Figure 6. Multiple comparisons of scale parameters for each processed image

of the neuro coil algorithm. In a previous study, the iMAR algorithm for large metal implants was more effective in reducing artifacts than the unique site-specific iMAR algorithm.[11] However, in the present study, the iMAR algorithm for large metal implants, such as hip implants, was ineffective. Therefore, the present study highlights that the iMAR algorithm corresponding to sites where metal artifacts are expected to be strong or large is not always effective.

Notably, several similar previous studies have reported the importance of using a dedicated algorithm to obtain optimal results.[11] The generation of artifacts at the bone-metal boundary due to the use of the MAR algorithm,[12] underestimation of metal size,[4] reduction of artifacts, and secondary effects of new artifacts, such as the generation of new artifacts[4,15,26] have also been observed. Therefore, the method that best fits the situation should be selected, particularly when using iMAR for non-targeted metal artifacts, as in the present study. Furthermore, the iMAR of which implant is effective in reducing artifacts and can be applied should always be considered.

A possible reason for the lack of significant differences in the location parameters among the respective images is that the ROI settings were large for areas with prominent artifacts. If the plots contain many regions with small CT value differences between adjacent pixels, as in the present study, they are expected to be closer in the regions where the largest variation is small, as shown in **Figure 5**. This small value may have influenced the lack of significant differences in the location parameters. Therefore, we believe that it may be better to limit the size of the ROI to the area where the artifacts are most pronounced and evaluate it.

This study has some limitations. First, ECG electrodes were used as the extracorporeal metal, and only one location was considered. However, the electrodes could be affixed to several locations, and the location of the affixation is expected to vary. When the location of the electrodes is changed, the body part (organ) affected by the artifact may change, and the intensity and pattern of the artifact generation may also change. It is necessary to further examine whether the difference in the location of the electrodes affects artifact reduction when the iMAR is used. Second, only one type of ECG electrode was evaluated in this study. When attempting to use iMAR for metal artifacts generated from other ECG electrodes, it may be necessary to consider which iMAR algorithm can be applied, as the pattern of artifact generation is expected to vary depending on the product and material used. However, if the pattern of generated artifacts and the background structure match the conditions for the use of a particular iMAR algorithm, we believe that it is possible to consider different algorithms.

In the present phantom-based study, the Gumbel method was used to evaluate the metal artifacts. According to Imai et al., all variations resulting from artifacts in CT images follow the Gumbel distribution.[18] In previous studies on the quantitative evaluation of metal artifacts using the Gumbel method, streak artifacts, which are the main components of metal artifacts, were artificially generated and evaluated.[18-21] To date, no studies have evaluated the applicability of the method used in the present study to clinical images; however, its applicability to clinical images has been suggested.[22] Therefore, we plan to examine whether this evaluation method can be applied to clinical images, where CT values vary depending on the structure of the body owing to organs in the background of artifacts.

Conclusion

The iMAR algorithm may be effective in reducing artifacts outside of the preset range of use. In this study, a reduction in metal artifacts generated from ECG electrodes attached to the body was demonstrated. Therefore, iMAR may also be effectively used for metals outside the body. By verifying whether the iMAR can be applied to structures with complex backgrounds, such as clinical images, we expect that it will become even more valuable in the future.

Conflicts of interest

The authors have no relevant financial or non-financial interests to disclose.

Acknowledgements

We would like to express our deepest gratitude to Kanae Matsuura phD from Suzuka University of Medical Science for her generous guidance and advice on data analysis methods and analysis. We would also like to thank those who provided advice on this study.

References

1. Ichikawa K. CT super basic. Tokyo, Japan: Ohmsha; 2015.
2. Katsura M, Sato J, Akahane M, Kunimatsu A, Abe O. Current and novel techniques for metal artifact reduction at CT: practical guide for radiologists. Radiographics 2018;38(2):450-461. https://doi.org/10.1148/rg.2018170102
3. Greffier J, Larbi A, Frandon J, Daviau PA, Beregi JP, Pereira F. Influence of iterative reconstruction and dose levels on metallic artifact reduction: a phantom study within four CT systems. Diagn Interv Imaging. 2019;100(5):269-277. https://doi.org/10.1016/j.diii.2018.12.007
4. Huang JY, Kerns JR, Nute JL, et al. An evaluation of three commercially available metal artifact reduction methods for CT imaging. Phys Med Biol. 2015;60(3):1047-1067. https://doi.org/10.1088/0031-9155/60/3/1047
5. Selles M, van Osch JAC, Maas M, Boomsma MF, Wellenberg RHH. Advances in metal artifact reduction in CT images: A review of traditional and novel metal artifact reduction techniques. Eur J Radiol. 2024;170:111276. https://doi.org/10.1016/j.ejrad.2023.111276
6. Hauser TK, Oergel A, Hurth H, Ernemann U, Seeger A. Artifact reduction in the diagnosis of vasospasm in computed tomographic perfusion: potential of iterative metal artifact reduction. J Comput Assist Tomogr. 2019;43(4):553-558. https://doi.org/10.1097/rct.0000000000000879

7. Aissa J, Boos J, Sawicki LM, et al. Iterative metal artifact reduction (MAR) in postsurgical chest CT: comparison of three iMAR-algorithms. Br J Radiol. 2017;90(1079):20160778. https://doi.org/10.1259/bjr.20160778
8. Pagniez J, Legrand L, Khung S, et al. Metal artifact reduction on chest computed tomography examinations: comparison of the iterative metallic artifact reduction algorithm and the monoenergetic approach. J Comput Assist Tomogr. 2017;41(3):446-454. https://doi.org/10.1097/rct.0000000000000544
9. Boomsma MF, Warringa N, Edens MA, et al. Quantitative analysis of orthopedic metal artifact reduction in 64-slice computed tomography scans in large head metal-on-metal total hip replacement, a phantom study. Springerplus. 2016;5:405. https://doi.org/10.1186/s40064-016-2006-y
10. Pan YN, Chen G, Li AJ, et al. Reduction of metallic artifacts of the post-treatment intracranial aneurysms: effects of single energy metal artifact reduction algorithm. Clin Neuroradiol. 2019;29(2):277-284. https://doi.org/10.1007/s00062-017-0644-2
11. Aissa J, Thomas C, Sawicki LM, et al. Iterative metal artifact reduction in CT: can dedicated algorithms improve image quality after spinal instrumentation? Clin Radiol. 2017;72(5):428.e7-428.e12. https://doi.org/10.1016/j.crad.2016.12.006
12. Neroladaki A, Martin SP, Bagetakos I, et al. Metallic artifact reduction by evaluation of the additional value of iterative reconstruction algorithms in hip prosthesis computed tomography imaging. Medicine (Baltimore). 2019;98(6):e14341. https://doi.org/10.1097/md.0000000000014341
13. Hoyoshi K, Satou T, Okada A. [Effect of hybrid iterative reconstruction on CT image quality using metal artifact reduction]. Nihon Hoshasen Gijutsu Gakkai Zasshi. 2018;74(8):797-804. Japanese. https://doi.org/10.6009/jjrt.2018_jsrt_74.8.797
14. Takayanagi T, Arai T, Amanuma M, et al. [Pacemaker-induced metallic artifacts in coronary computed tomography angiography: clinical feasibility of single energy metal artifact reduction technique]. Nihon Hoshasen Gijutsu Gakkai Zasshi. 2017;73(6):460-466. Japanese. https://doi.org/10.6009/jjrt.2017_jsrt_73.6.460
15. Nagayama Y, Tanoue S, Oda S, et al. Metal artifact reduction in head CT performed for patients with deep brain stimulation devices: effectiveness of a single-energy metal artifact reduction algorithm. AJNR Am J Neuroradiol. 2020;41(2):231-237. https://doi.org/10.3174/ajnr.a6375
16. Tsuboi K, Fukunaga M, Yamamoto H. [The effect of metal artifact reduction at different calibrated and display field of views in computed tomography]. Nihon Hoshasen Gijutsu Gakkai Zasshi. 2016;72(12):1237-1244. Japanese. https://doi.org/10.6009/jjrt.2016_jsrt_72.12.1237
17. Takada K, Ichikawa K, Banno S, Otobe K. [Suggestion of the relative artifact index for noise-independent evaluation of the streak artifact]. Nihon Hoshasen Gijutsu Gakkai Zasshi. 2018;74(4):315-325. Japanese. https://doi.org/10.6009/jjrt.2018_jsrt_74.4.315
18. Imai K, Ikeda M, Wada S, et al. Analysis of streak artifacts on CT images using statistics of extremes. Br J Radiol. 2007;80(959):911-918. https://doi.org/10.1259/bjr/93741044
19. Nakamura S, Kawata H, Kuroki H, Mizoguchi A. [Effect of reconstruction technique for metal artifact reduction in computed tomography by changing display field of view]. Nihon Hoshasen Gijutsu Gakkai Zasshi. 2015;71(11):1096-1102. Japanese. https://doi.org/10.6009/jjrt.2015_jsrt_71.11.1096
20. Kitaguchi S, Imai K, Ueda S, et al. [Quantitative evaluation of metal artifacts on CT images on the basis of statistics of extremes]. Nihon Hoshasen Gijutsu Gakkai Zasshi. 2016;72(5):402-409. Japanese. https://doi.org/10.6009/jjrt.2016_jsrt_72.5.402
21. Nakane J, Kobayashi Y, Shiozawa T. [Isotropic evaluation of streak artifact using extreme value statistical analysis]. Nihon Hoshasen Gijutsu Gakkai Zasshi. 2015;71(12):1165-1173. Japanese. https://doi.org/10.6009/jjrt.2015_jsrt_71.12.1165
22. Nomura Y, Watanabe H, Manila NG, Asai S, Kurabayashi T. Evaluation of streak metal artifacts in cone beam computed tomography by using the Gumbel distribution: a phantom study. Oral Surg Oral Med Oral Pathol Oral Radiol. 2021;131(4):494-502. https://doi.org/10.1016/j.oooo.2020.08.031
23. Imai K, Ikeda M, Enchi Y, Niimi T. Quantitative assessment of image noise and streak artifact on CT image: comparison of z-axis automatic tube current modulation technique with fixed tube current technique. Comput Med Imaging Graph. 2009;33(5):353-358. https://doi.org/10.1016/j.compmedimag.2009.02.003
24. Imai K, Ikeda M, Enchi Y, Niimi T. Statistical characteristics of streak artifacts on CT images: relationship between streak artifacts and mA s values. Med Phys. 2009;36(2):492-499. https://doi.org/10.1118/1.3056554
25. Ishikawa T, Suzuki S, Harashima S, Fukui R, Kaiume M, Katada Y. Metal artifacts reduction in computed tomography: A phantom study to compare the effectiveness of metal artifact reduction algorithm, model-based iterative reconstruction, and virtual monochromatic imaging. Medicine (Baltimore). 2020 11;99(50):e23692. https://doi.org/10.1097/md.0000000000023692
26. Wayer DR, Kim NY, Otto BJ, Grayev AM, Kuner AD. Unintended consequences: review of new artifacts introduced by iterative reconstruction CT metal artifact reduction in spine imaging. AJNR Am J Neuroradiol. 2019;40(11):1973-1975. https://doi.org/10.3174/ajnr.a6238